We are IntechOpen,
the world's leading publisher of
Open Access books
Built by scientists, for scientists

4,800
Open access books available

122,000
International authors and editors

135M
Downloads

Our authors are among the

154
Countries delivered to

TOP 1%
most cited scientists

12.2%
Contributors from top 500 universities

CLARIVATE ANALYTICS
BOOK CITATION INDEX
INDEXED

WEB OF SCIENCE™

Selection of our books indexed in the Book Citation Index
in Web of Science™ Core Collection (BKCI)

Interested in publishing with us?
Contact book.department@intechopen.com

Numbers displayed above are based on latest data collected.
For more information visit www.intechopen.com

Structural and Thermoelectric Properties Characterization of Individual Single-Crystalline Nanowire

Dedi, Indah Primadona, Ping-Chung Lee,
Chi-Hua Chien and Yang-Yuan Chen

Additional information is available at the end of the chapter

Abstract

Herein, we report a method for structural characterization as well as TE properties measurements of individual single-crystalline Lead telluride (PbTe) NWs by employing a new microchip design. In this work, the single PbTe NW was characterized in four different types of measurement: structural characterization, Seebeck coefficient S, electrical conductivity σ, and thermal conductivity κ. The structural characterization by transmission electron microscope (TEM) revealed that the PbTe NWs were high-quality single crystals with a growth along the [100] direction. The TE properties S, σ, and κ measurement results of individual 75 nm PbTe NW at room temperature were −54.76 µV K^{-1}, 1526.19 S m^{-1}, and 0.96 W m^{-1} K^{-1}, respectively. Refer to the result of S, σ and κ; the figure of merit ZT values of a 75 nm PbTe NW at the temperature range of 300–350 K were 1.4–4.3 x 10^{-3}. Furthermore, it was observed that the κ value is size-dependent compared to previous reported, which indicates that thermal transport through the individual PbTe NWs is limited by boundary scattering of both electrons and phonons. The results show that this new technique measurement provided a reliable ZT value of individual NW yielded high accuracy for size-dependent studies.

Keywords: lead telluride, nanowires, thermal conductivity, size-dependent, figure of merit

1. Introduction

Recently, nano-engineered thermoelectric (TE) materials used for converting waste heat into electricity have become an interesting research topic. TE energy converters are devices that

can harvest renewable energy for power generation and thermal sensing application [1–3]. The efficiency of TE materials is evaluated based on the dimensionless figure of merit ZT, which is written as $S^2\sigma T/(\kappa_e + \kappa_l)$, where S, σ, κ_e, and κ_l denotes the thermal power or Seebeck coefficient, the electrical conductivity, the electronic thermal conductivity, and the lattice thermal conductivity, respectively. The quantity of $S^2\sigma$ is defined as the power factor (PF). Theoretically, a reduction in dimensionality from three dimensions to one dimension yields a dramatically increased electronic density of states (DOS) at the energy band edges and a decreased thermal conductivity. As a result, the thermoelectric PF and assuredly ZT value enhances [4, 5]. Numerous studies have reported that the enhancement of ZT value in nano-materials is the result of quantum confinement effects and increased surface phonon scattering [3, 6, 7].

Due to the nanometer scale effect, it is believed that in NWs comprising TE materials, such as PbTe, the value of S is higher than its bulk counterpart [8, 9]. According to the certain carrier-scattering assumptions, the enhancement of S value occurs because of the sharp increase in the local DOS around the Fermi level, which also can be interpreted as an increased local DOS effective mass ($m_d{}^*$). However, with the overall benefit of such an improvement in S, nanosize will cause a declining in carrier mobility (μ) and thus affect to the decreasing the ZT value. This is occurs because the increased local DOS usually leads to a heavier trans-port-effective mass of carriers. In the most well-known high-temperature TE, the carriers are predominantly scattered by phonons. [10] Increasing the S is an obvious goal for obtaining a high efficiency TE materials. Nevertheless, other changes in transport properties often sacrifice the σ correlated with an increase in the S and thus do not ultimately lead to an improvement in ZT.

In order to unveil the size effect on the intrinsic physical properties of TE materials, the mea-surement of nanowire without interference from either the matrix or external contacts is imperative. Furthermore, the TE properties measurement as well as structural characteriza-tion on single nanowire is also crucial in terms of the accuracy and reliability of the resulting ZT value. The low accuracy may occur because every single nanowire, although in the same batch synthesis process, may have a different structure or TE properties. However, measuring all properties on single nanowire is still challenging due to the unavailability of NW micro-chip which is compatible for all type measurements.

In this chapter, the synthesis and structural characterization of PbTe NWs as well as the prep-aration of newly design NW's microchip to resolve the above mentioned problem will be described in the first section. For synthesizing the NW, an alternative free-catalyst technique, the stress-induced growth method will be introduced. In the second section, we will discuss about their TE properties (S, σ, and κ).

Type of TE NW used in this chapter was single-crystalline PbTe NW. PbTe is a semiconductor with an energy band gap of 0.31 eV at 300 K [11–14]. In recent years, it has been found that PbTe is one of the superior TE materials in the temperature range of 400–900 K. This material has a large Seebeck coefficient, a very low κ_l (2.2 W m^{-1} K^{-1} at 300 K) [15] and a good electrical conductivity when appropriately chemical doped [16]. The synthesis of low-dimensional PbTe NWs has been

intensively explored in the past decades [17–27]. Besides that, there have also been some studies on the TE properties of PbTe-based nanostructures such as PbTe/PbSeTe quantum dot superlattice [28] and PbTe NWs [20] with room temperature ZT value 0.75 and 0.0054, respectively.

2. Synthesis and structural characterization of PbTe NWs

2.1. Synthesis of PbTe NWs

In this work, the synthesis of single-crystalline PbTe NWs via a stress-induced method is described elsewhere [27], in a way similar to the on-film formation (ON–OFF) growth of other semiconductor NWs. [29] Briefly, the PbTe was made by mixing elemental Pb (Alfa Aesar, −200 mesh, 99.9%) and Te (Alfa Aesar, −325 mesh, 99.999%) inside a carbon-coated silica tube. After that, the resulting mixtures inside the tube was vacuumed up to 10^{-6} Torr, sealed, and slowly heated to 1000°C over a period of 12 hours. On the top of the heating process, the temperature was held for 4 hours, and then cooled down to room temperature. The resulted ingot was then cut by a diamond saw into a disc shape with a diameter of 10 mm. Before fabricating the PbTe films, the disc target and substrates were both ultrasonically cleaned in acetone, isopropanol, and then rinsed with deionized water. The PbTe films were prepared by depositing the synthesized PbTe ingot on single-crystal SiO_2/Si (100) substrates in a pulsed laser deposition (PLD) system (LPX Pro 210). The base pressure of the vacuum system was 5.0×10^{-7} Torr. The excimer laser was applied for 15 min at room temperature with energy and frequency of 140 mJ and 10 Hz, respectively. The substrate rotation speed was approximately 10 rpm. With the all mentioned set up, the total thickness of the PbTe films was about 20 nm. To synthesis PbTe NWs, the PbTe films were sealed in a vacuumed quartz tube below 5×10^{-6} Torr, annealed at 450°C for 5 days, and then cooled slowly to room temperature. During the annealing process, the NWs grew from the film to release the compressive stress caused by the difference in thermal expansion coefficients between the PbTe film (19.8×10^{-6}/°C) and the SiO_2/Si substrate (0.5×10^{-6}/°C)/(2.4×10^{-6}/°C).

2.2. Microchip preparation

As mentioned above, the challenge in working with TE NW was the measurement of thermoelectric properties as well as structural analysis on specific single-crystalline nanowire, to get a high accuracy of ZT value. Here, in order to solve that problem, a novel design of microchip was discussed. The preparation processes of the measurement platform are shown in **Figure 1**. First, the silicon (Si) wafer with Si_3N_4 layer (**Figure 1a**) on both sides was covered with the photoresist by using spin coating method (**Figure 1b**), followed by standard photolithography processes. After that the exposure soluble photoresist can be developed by the developer. The Si wafer was then put into the reactive ion etching system (RIE, Model: ANELA DEM-451T) for dry etching. The unprotected Si_3N_4 will be etched by the reactive ion. Then, the wafer is immersed into potassium hydroxide (KOH) solution for wet etching. The silicon which is exposed to KOH will be etched and leaving a thin Si_3N_4 membrane for further processes.
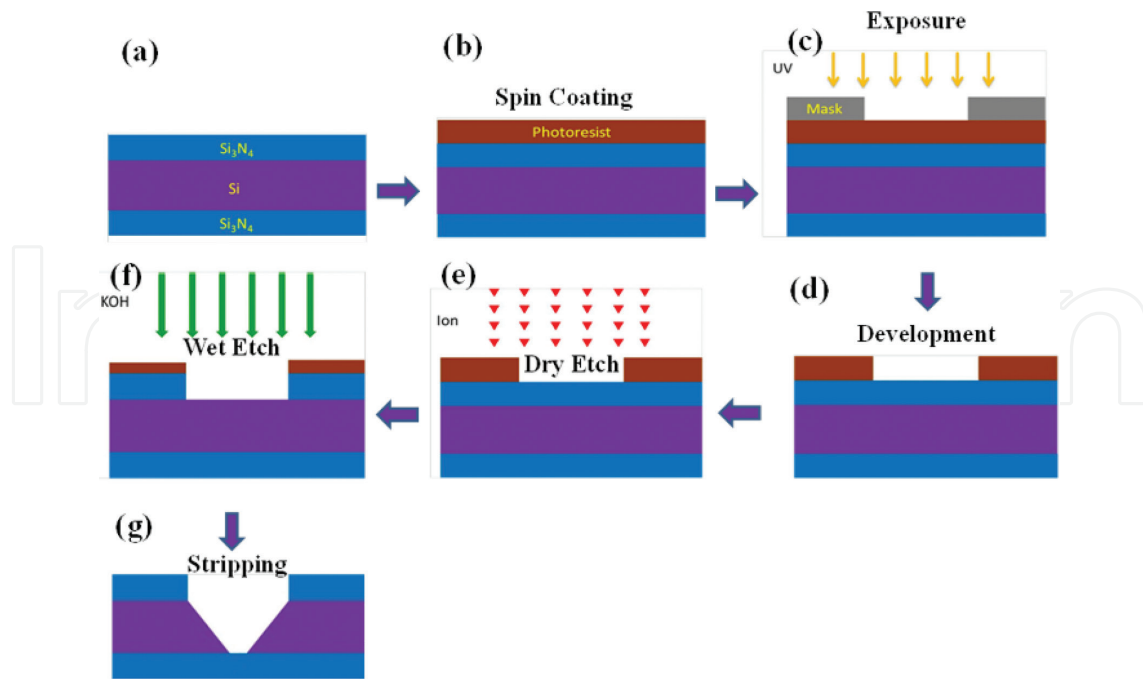
Figure 1. Schematic Si$_3$N$_4$ membrane template preparation: (a) the silicon wafer with Si$_3$N$_4$ on the both sides, (b) substrate is spin coated with photoresist, (c) Photoresist is exposed to a rectangular pattern with ultraviolet light, (d) soluble photoresist can be developed by the developer, (e) removing Si$_3$N$_4$ layer by reactive ion etching system (RIE), (f) dip the wafer into a bath of KOH for wet etching to create a cavity and leave a suspended Si$_3$N$_4$ membrane, and (g) strip the photoresist.

The standard photolithography processes were used to define the contact pads of the measurement platform. As shown in **Figure 2**, first, Si wafer with Si$_3$N$_4$ membrane is covered with photoresist material by spin coating, followed by exposure, evaporation, and lift-off process. The developed primary measurement platform is then ready to be used.

The flow chart of the suspending process of a nanowire on the measurement platform (microchip) was shown in **Figure 3**. Resistance temperature detectors (RTDs) and current leads were fabricated on the primary measurement platform by electron beam lithography [E-Beam Writer System, Model: Elionix ELS-7000 (100 keV)]. The Si$_3$N$_4$ membrane was removed by inductively coupled plasma etching system (ICP, Model: Elionix EIS-700) to open the window. After that, the single nanowire from the PbTe thin film was picked up by a tungsten needle (dw = 100 nm) under a binocular optical microscope and placed across on two RTDs of a Si$_3$N$_4$ microchip, where both ends of the nanowire attached to the current leads. In order to improve thermal and electrical contacts between the nanowire and the contact pads, the contacts of the nanowire on thermometers and current leads were covered with a thin layer of Platinum (Pt) using a focused ion beam (FIB) [DBFIB-SEM, FEI NOVA-600].

To examine how good the prepared contact, the contact resistance of all four points (point 1, 2, 3, and 4) as depicted in **Figure 4** were measured. First, the known direct current (DC) was applied between contacts 1 and 4 (4 probes) and then the voltage drop across contact 2 and 3 (2 probes, see **Figure 4**) was measured. The total resistance of two-point probe configuration is expressed as $R_{2point} = R_{lead} + 2R_{contact} + R_{nw}$. Wherein, R_{2point}, R_{lead}, $R_{contact}$, and
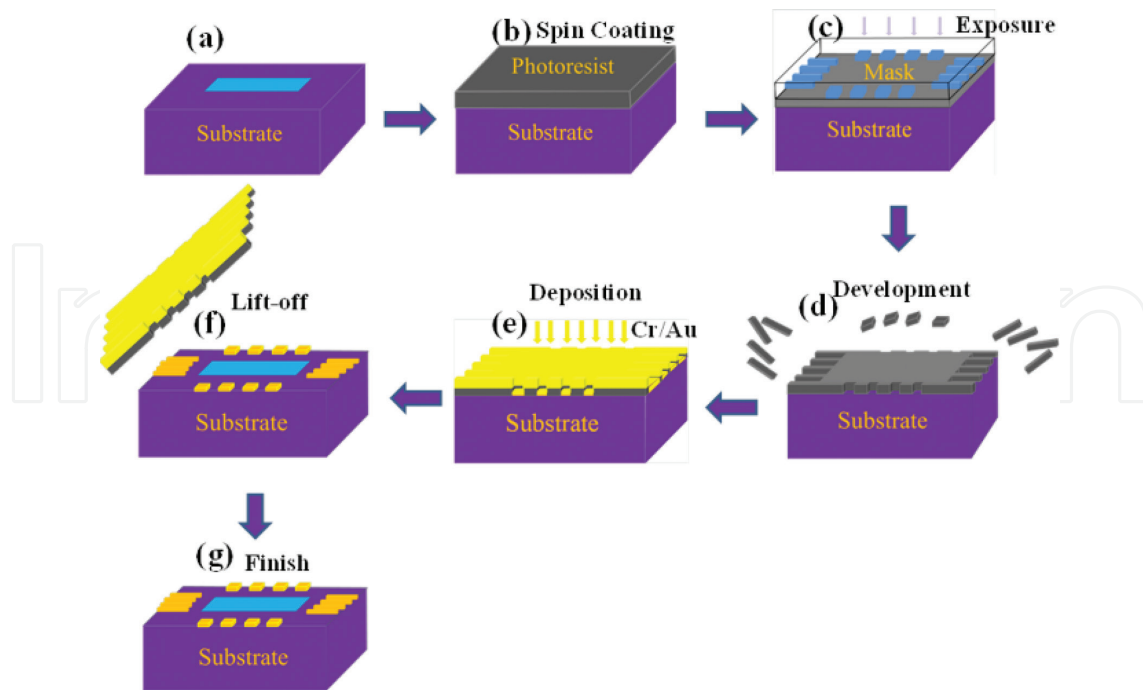
Figure 2. Schematic of depositing outer electrodes of the template: (a) silicon wafer with Si_3N_4 membrane, (b) substrate is spin coated with photoresist, (c) photoresist can be exposed to a pattern by ultraviolet light, (d) soluble photoresist will be developed by the developer, (e) the Cr/Au electrodes are deposited by thermal evaporator, (f) lift-off the photoresist by acetone, and (g) measurement platform is ready to be used.

R_{nw} represents resistance between point 2 and 3, resistance of Cr/Au electrodes, resistance of contacted NW to electrode, and NW resistance, respectively. The resistance of R_{2point} and R_{nw} were measured by two and four-point probes. Whilst, in order to obtain the contact resistance as $R_{cont} = (R_{2point} - R_{nw})/2$, R_{lead} (~10 Ω) was neglected. The measurement result of R_{2point} was about 6–7% from R_{nw} value. Since the power dissipation at the contacts is much smaller than the minimum power for 3ω signal, the resultant contact resistance supposedly does not affect the third harmonic signal. Furthermore, the contact metal pads act as large thermal reservoirs where the temperature is kept constant at the initial temperature during the experiment.

In addition, the prepared nanowire exhibited a linear current–voltage (I-V) curve wherein indicated the Ohmic contact response; the current range within 0 to 100 µA indicating the resistivity of NW follows the Ohm's law. An Ohmic contact is an electrical junction between two conductors which has a linear current–voltage (I-V) curve following the Ohm's law. Low resistance Ohmic contacts are applied to facilitate the flow of charge in both directions between the two conductors, without blocking from the excess power dissipation due to voltage thresholds. The contact quality has a contribution to both an electrical and a thermal effect, such as, if the electrical contact resistance is too high, the third harmonics measurement will be influenced by the heat dissipation occurred at the contacts due to Joule heating. Furthermore, incorrect selection of a working frequency will develop an error experiment results. Therefore, the AC impedance measurements with no electrical artifacts involved were utilized to choose a correct working frequency.
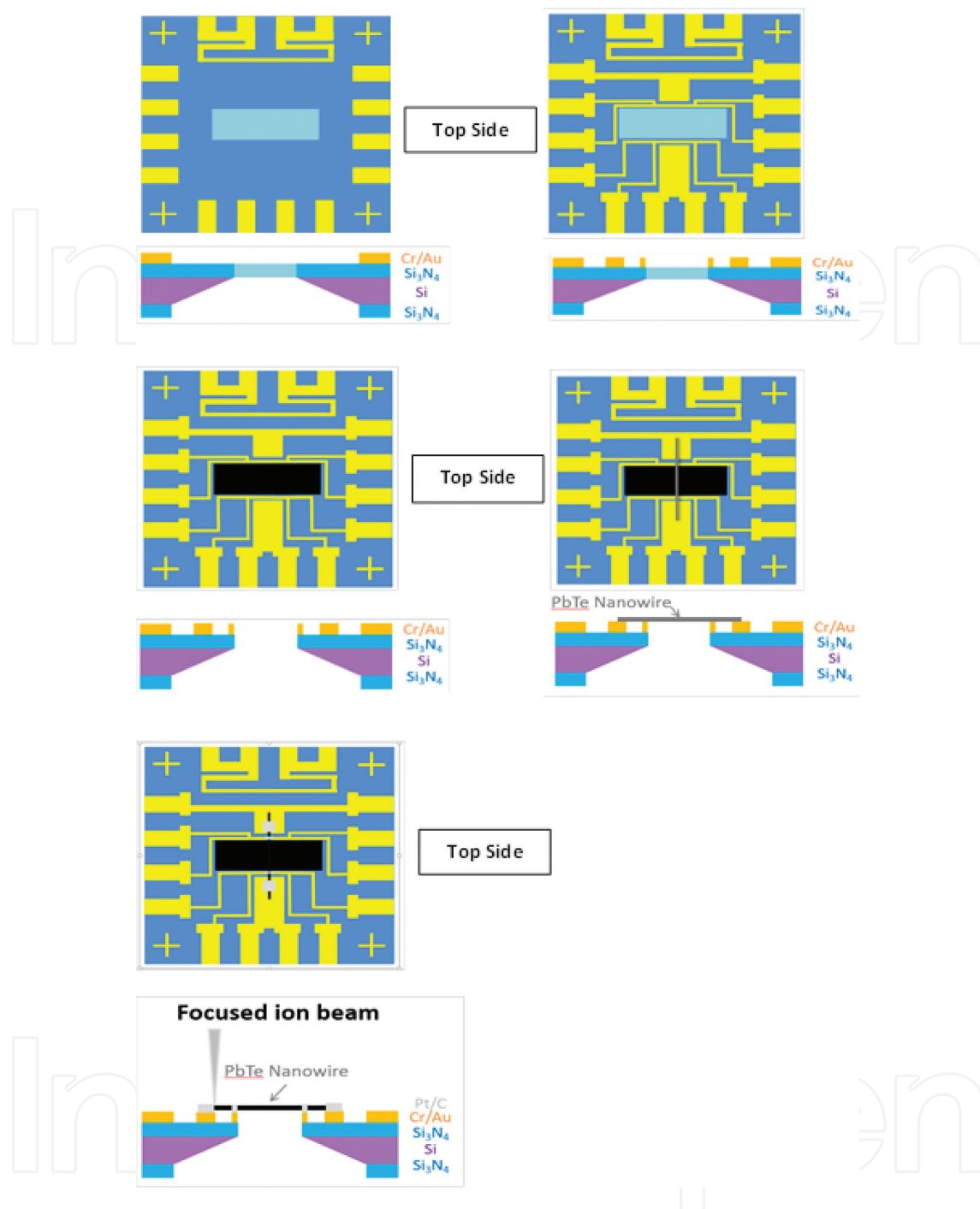
Figure 3. Flow charts of the suspending process of a nanowire on the measurement platform.

2.3. Structural characterization of PbTe NWs

The size and crystalline structure of PbTe NWs were characterized by scanning electron microscope (SEM) and transmission electron microscope (TEM). The SEM image of grew PbTe NWs on the substrate (**Figure 5a**) reveals that the length and the diameter of NWs were ranging from 5 to 70 μm and 50 to 300 nm, respectively. The NWs with length about 70 μm was picked up, placed, and contacted on the microchip as shown in **Figure 5b**. The prepared contacts have a
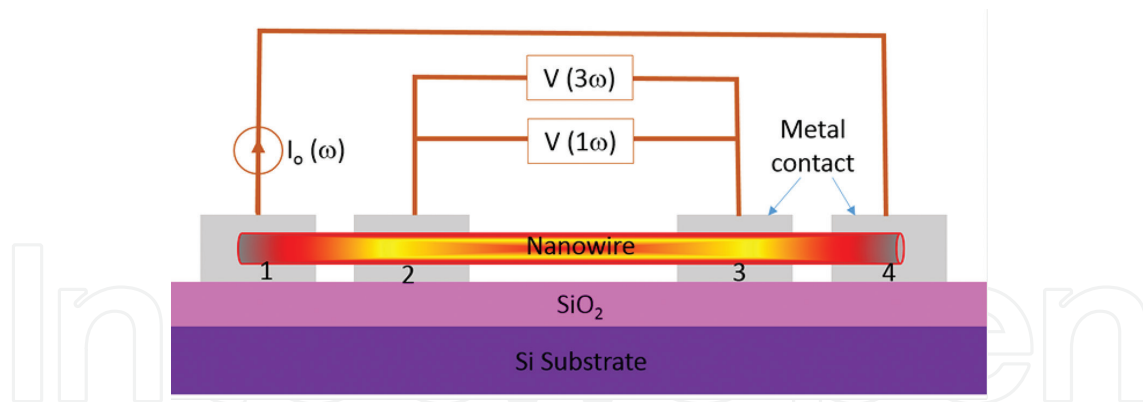
Figure 4. A schematic setup of four-point probe for measurement of electrical resistance (R), Seebeck coefficient (S) and the thermal conductivity (κ) by 3ω method.
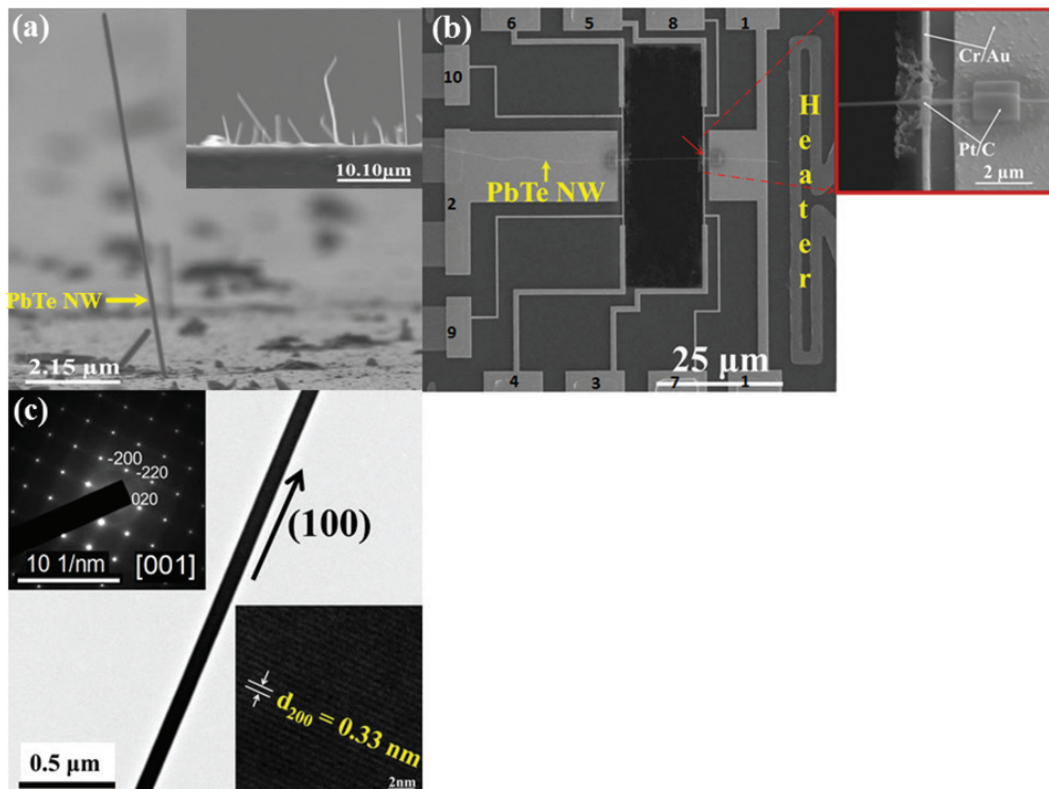

Figure 5. (a) SEM image of PbTe NWs grew on the surface of the PbTe thin film, (b) SEM images of a PbTe NW suspended on a Si_3N_4 template, inset: the Pt/C thermal contact between the PbTe NW and 10-nm Cr/50-nm Au electrodes on a Si_3N_4 microchip, (c) low-magnification TEM images of a PbTe NW, inset of the top left of figure: the SAED pattern (at the [001] zone axis), inset of the bottom right of figure: a high-resolution TEM image of a PbTe NW.

resistance about 425–430 Ω, wherein showed nearly Ohmic contacts. The microchip consisting of PbTe NW displayed in **Figure 5b** was used for complete structural analysis and TE properties measurements. The representative TEM image showed that the employed PbTe NWs has a diameter of 75 nm (**Figure 5c**) and this size was further convinced by the scanning transmission electron microscope (STEM) result (**Figure 6a**). In addition, the TEM image and a corresponding selected-area electron diffraction (SAED) pattern (inset of the top left of **Figure 5c**) revealed
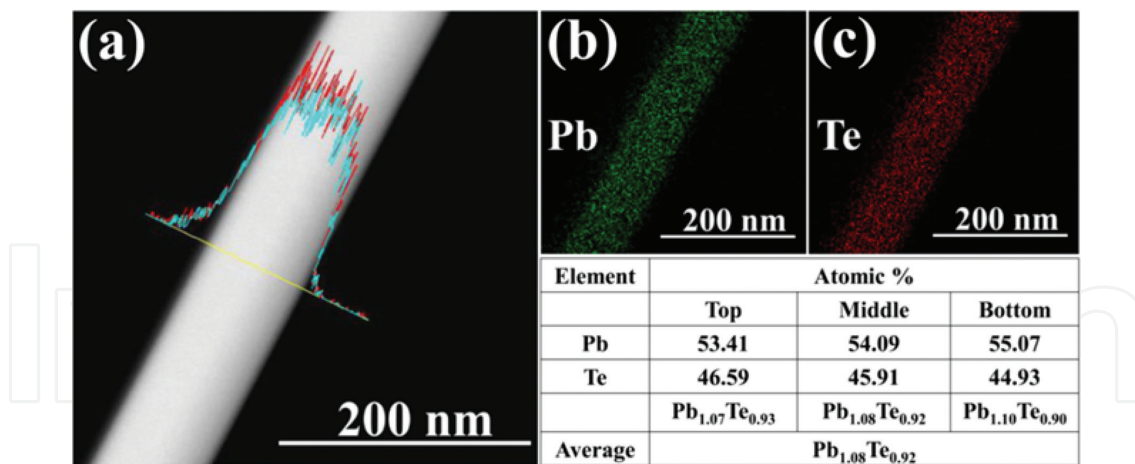
Figure 6. (a) STEM images of a PbTe NW. The line profiles show that the Pb (blue line) and Te (red line) are homogeneously distributed throughout the NW, (b) and (c) elemental mapping showing the uniform distribution of Pb and Te along the NW, respectively.

that the PbTe NWs were high-quality single crystals with a growth along the [100] direction. While, the lattice fringes of the smooth PbTe were separated by 0.33 nm (inset of the bottom right of **Figure 5c**). This is consistent with a periodicity along the [200] direction with lattice constants of approximately 6.549 Å, which are approximately 1.2% higher than the bulk counterpart (a = 6.47 Å).

The chemical composition of the PbTe NWs was studied by using energy dispersive X-ray spectroscopy (EDS). The EDS line scan profile, shown in **Figure 6a**, revealed the uniform spatial distribution of the Pb and Te elements throughout the NW. This was further confirmed by using a STEM to map elements across the NW [**Figure 6b** and **c**]. The EDS point scanning experiments of the NWs quantitatively confirmed that Pb and Te are present in an average atomic ratio of 54.19 and 45.81% (Table in **Figure 6**), respectively. In addition, the EDS data also revealed that the atomic ratio of Pb/Te ≈ 1.18, with no impurities. As a result, the stoichiometric composition of the individual NW was $Pb_{1.08}Te_{0.92}$.

3. Thermoelectric properties

As mentioned before that the microchip with a rectangular window which shown in **Figure 5b** was employed to measure the TE properties of NW, i.e. electrical resistivity (ρ) and Seebeck coefficient (S). In this experiment, the PbTe NW was placed across two resistance thermometers, hot side thermometer Th (a gold wire parallel line to the heater between contact electrodes 7 and 8 which is marked as red arrows in **Figure 5b**) and cold side thermometer Tc (a gold wire between the contact electrode 9 and 10, **Figure 5b**) with both ends of the NW attach to the current leads (electrode 1 and 2, **Figure 5b**). To measure the V1ω and V3ω signal, electrodes 3 and 4 (voltage leads) were connected to lock-in amplifier. The thermal conduction
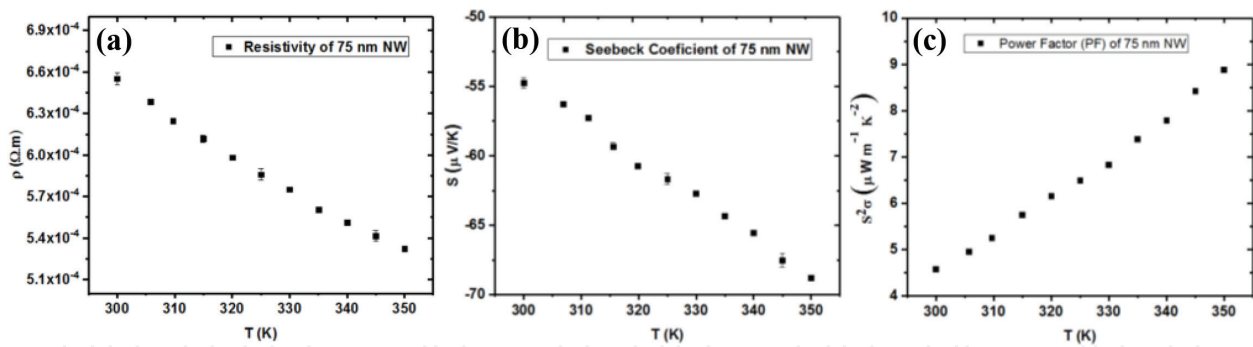
Figure 7. Temperature dependence of (a) electrical resistivity, (b) Seebeck coefficient, and (c) power factor of a 75 nm PbTe NW.

from NW to the microchip substrate that affects the S and ρ measurement was assured zero. Furthermore, in order to eliminate convectional heat loss, all measurements were carried out in a high vacuum of at least lower than 2×10^{-6} Torr.

Four-point probe method was applied for ρ measurement. In this work, an AC current flowed to the NW via electrode 1. The voltage (V) and current (I) difference between electrode 1 and 2 was measured through the voltage leads. A pair of current leads into the NW to determine the root mean square of the voltage difference of a pair of voltage leads. By substituting the obtained V and I value to the V = I•R formula, the resistance (R) value is obtained. We get the R of NW, the ρ value could be attained by applying the formula of ρ = R•A / L where A and L are cross-section area of the wire and length between a pair of voltage leads, respectively. **Figure 7a** showed the measurement results of NW resistivity ρ at temperatures range 300–350 K. This figure demonstrated that the resistivity ρ of a 75-nm PbTe NW was temperature dependence which indicated a semiconducting behavior. The resistivity of a PbTe NW at near room temperature was 6.55×10^{-4} Ω m, which 43 times greater than the bulk counterpart (1.52×10^{-5} Ω m) [14]. This is probably due to the surface scattering of charge carriers [30].

For the Seebeck effect measurement, the characterization was based on the voltage and temperature difference generated between electrodes 3 and 4 (**Figure 5b**). To generate the temperature gradient between those two electrodes, the heater with frequency 1ω and magnitude equals to I•$Sin(\omega t)$ was applied at one end of the NW. In this experiment, the sample was employed as the sensor of the thermometer as well, thus, temperature coefficient of electrical resistance of them are needed to be calibrated at first. By applying a DC current to the sensor and measuring the change of the voltage difference at frequency 2ω between the two ends of the sensor, the resistance change of the sensor would be known. After obtaining the temperature coefficient of electrical resistance, the temperature gradient created between two ends of the NW would be gained, because the observed heat is proportional to the square of the current multiplied by the electrical resistance of the NW, Q ∝ I^2•$sin^2(\omega t)$•R, where Q and R denote the observed heat and the electrical resistance of the NW, respectively. Mathematically, $sin^2\alpha = [(1-cos2\alpha)/2]$, it means that the frequency of 2ω was applied to heat the heater. As the heater is heated at frequency 2ω, the sample temperature and sensor resistance would fluctuated at frequency 2ω as well. By

knowing the temperature gradient and also measuring the thermoelectric voltage of two ends of the sample, S can be calculated by implementing the formula: $S = (\triangle V) / (\triangle T)$.

The experiment results of Seebeck effect of a 75-nm PbTe NW shown in **Figure 7b** revealed that the S value was temperature dependence. The S value increased with increasing the temperature. In addition, as depicted in **Figure 7b** that the S of PbTe NWs at various temperature measurements has a negative sign which indicated for n-type semiconductor material. Those negative sign appears because their electrons have a much higher µ than holes and dominate the electronic transport properties [31, 32]. At temperature of 300 K, the S value for the 75-nm NW was −54.76 µV K⁻¹, which is about 69% lower compare to the bulk counterpart [14]. This result may due to the consequences of structural imperfections, such as antisite defects inside PbTe NW (i.e., the creation of one vacancy at the tellurium site) [14, 33].

Theoretically, for almost all materials, the trend of ρ was closely correlated with the S. It was consistent with our experimental resultts (**Figure 7a** and **b**) which showed that the smaller ρ had a higher S value. Conversely, due to s = 1/ρ, thus s value increases when S is increased. The PF ($S^2\sigma$) calculation results of PbTe NWs as a function of temperature are plotted in **Figure 7c**. The PF increased gradually when the temperature increased, and this result was mainly due to the influence of ρ trends. At the temperature about 300 K the $S^2\sigma$ values were 4.58 µW m⁻¹ K⁻².

Comparing the S value as a function of carrier density of various PbTe bulk obtained by Harman et al., **Figure 8** show that the S was closely correlated with the carrier concentration (n), Our results was consistent with the other previous experiments [14, 34] in which a smaller n had a higher S value.
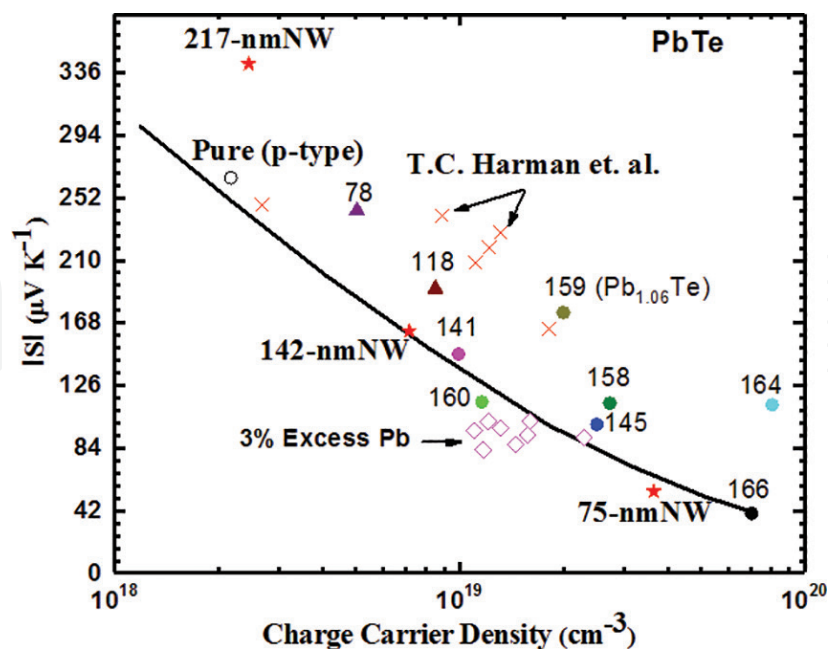

Figure 8. Absolute value of the thermoelectric power or Seebeck coefficient (S) of various PbTe samples [14] as a function of carrier density; electrons (n) or holes (h) at room temperature. The solid red stars denote the $Pb_{1.08}Te_{0.92}$ samples with 75, 142, and 217 nm diameter wires [27, 34].
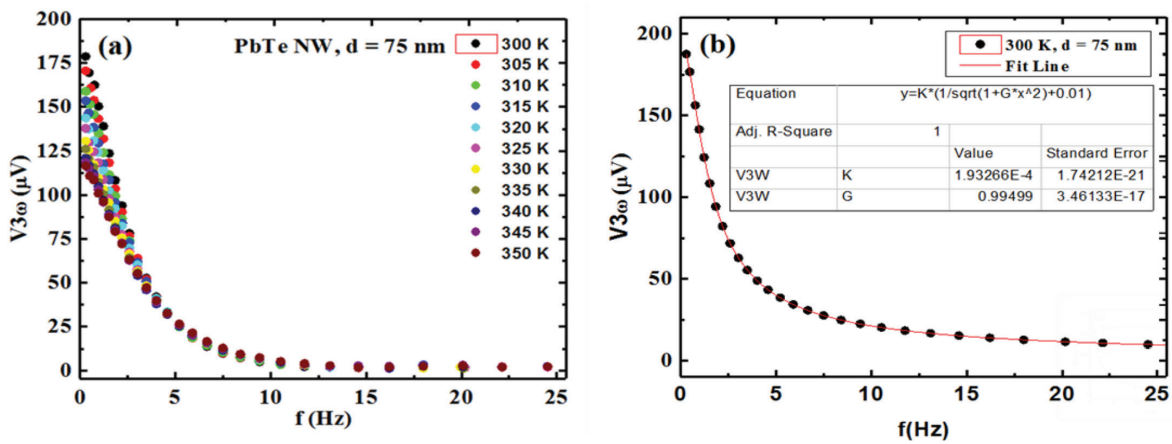
Figure 9. (a) Frequency dependence of $V_{3\omega}$ at 300–350 K for 75 nm PbTe NW and (b) the solid line is predicted relation $V_{3\omega} \propto 1/\sqrt{(1 + (2\omega\gamma)^2)}$ at 300 K for a 75 nm PbTe NW.

The thermal conductivity of the 75 nm PbTe nanowire was measured by the self-heating 3ω method [35] in the temperature range of 300–350 K. In the experiment, the $V_{3\omega}$ as a function of frequency will be attained. As shown in **Figure 9a**, the $V_{3\omega}$ was dependent on the frequency. The $V_{3\omega}$ reduce significantly by increasing the frequency, however, the reduction become slightly at a frequency above 10 Hz. The relation between thermal conductivity, $V_{3\omega}$ and frequency is described in the Eq. (1).

$$V_{3\omega} = \frac{4\,I_0^3\,R\,R'\,L}{\pi^4\,\kappa S\,\sqrt{1 + (2\omega\gamma)^2}} \tag{1}$$

which simplified as:

$$y = \frac{K}{\sqrt{1 + Gx^2}} \tag{2}$$

where I and ω denote the amplitude and frequency of the alternating current applied on nanowire, R and R' are the resistance and derivative of resistance at corresponding temperature, κ is the thermal conductivity, S is the cross section, and γ is the characteristic thermal time constant.

Figure 9b shows the fitting result of $V_{3\omega}$ to frequency of a 75 nm PbTe NW at 300 K. The thermal conductivity κ of the nanowire can be derived from the intercept of the fitting value at a certain temperature $V_{3\omega} = (4I_0^3LRR')/(\pi^4\kappa S)$ ($\omega\gamma \to 0$). To further validate the extraction of thermal conductivity by 3ω method, the variation of 3ω signals toward the input current amplitude I_0 and frequency was studied. The result shows that $V_3\omega$ versus I_0 follows the I_0^3, as exhibited in the equation of **Figure 10**, which mean it agree with the Eq. (1).

By substituting all acquired data from self-heating 3ω experiment to Eq. (1), the thermal conductivity, κ of a 75 nm PbTe NW at range temperature of 300–350 K were 0.96–0.72 Wm^{-1} K^{-1} (**Figure 11a** and **b**), which is approximately 2.40–3.19 times lower than the bulk counterpart (κ = 2.3 W m^{-1} K^{-1}). Likewise, the κ value at room temperature was 0.96 W m^{-1} K^{-1}, which is
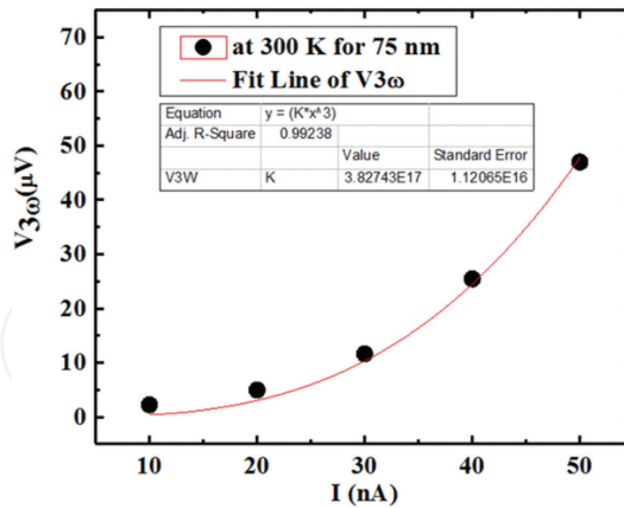
Figure 10. The 3rd harmonic voltage signal $V_{3\omega}$ as function of the extraction current amplitude I_0 for a 75 nm PbTe NW at 300 K. Red solid line represents the cubic relationship of $V_{3\omega}$ and I_0.

approximately 58% lower than the typical reported value of κ = 2.3 W m^{-1} K^{-1} for bulk PbTe. This decline mainly due to the carrier concentration difference or size effect. [36]

For the purpose of calculating the κ_l value, the electron thermal conductivity κ_e need to be determined. The κ_e value is calculated by using Eq. (3) (Wiederman-Franz law, where the Lorenz number L = 2.44 × 10^{-8} W.Ω.K^{-2}), while the κ_l is gained from subtracting the κ with κ_e value. The values of κ_l of a 75 nm PbTe NW at 300 K was 0.95 W m^{-1} K^{-1}, which is 57% lower than the PbTe bulk (κ_l = 2.2 W m^{-1} K^{-1}). [16] As reference, the lattice contribution (κ_l) of super-lattice thin films PbSe$_{0.98}$Te$_{0.02}$/PbTe at room temperature was 0.35 W m^{-1} K^{-1} [28].

$$\kappa_e = \text{L}.\sigma.\text{T} \tag{3}$$

The lattice thermal conductivity has a lower limit wherein the phonon mean free path becomes comparable to the lattice spacing of the atoms [37]. Alternatively, the lattice thermal conductivity of a material can be determined by using Eq. (4), where C, ν, and ι represent the heat capacity per unit volume, the speed of sound in the material, and the mean free path of the phonons, respectively. By applying the atom spacing of PbTe as the minimum ι and substituting the values of the ν and C to Eq. (4), the κ_l of PbTe is around 0.2 W m^{-1} K^{-1}. Repeating this calculation for a variety of compounds, the lowest possible value of κ_l are in the range of 0.1–0.2 W m^{-1} K^{-1} [38].

$$\kappa_l = 1/3.\text{C}.\nu.\iota \tag{4}$$

As the size of the nanowire approaches the ι (the median phonon free path in PbTe is about 42 nm) [39], the κ value will drop due to the increased phonon scattering. According to the reported κ of individual PbTe NW with various diameters (d = 182, 277, and
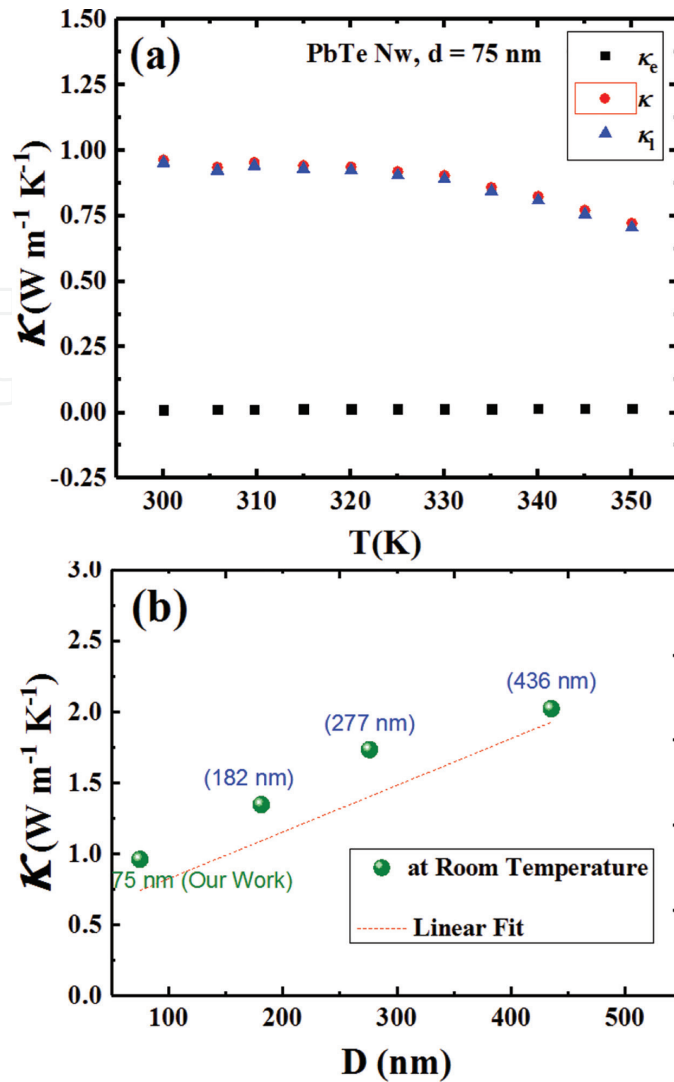
Figure 11. (a) Measured thermal conductivity κ(●), electron thermal conductivity κ_e (■) and lattice thermal conductivity κ_l (▲) of a 75 nm PbTe NW and (b) size-dependent κ properties of individual 75 nm PbTe NW (compared to the reported 182 nm, 277 nm and 436 nm [19].

436 nm) [19] including our recent work (d = 75 nm) which were plotted in **Figure 11b**, the κ value decreases gradually as its diameter shrinks. The enhanced phonon boundary scattering has a considerable effect in reducing the κ value of NW. Hence, it is suggested to have an effect on suppressing the phonon transport through the NWs as well [40, 41]. Theoretically, those phenomena would cause the ZT value of NW higher than the bulk counterpart, provided that the electronic properties were not degraded by the nanostructure. However, based upon all the above measurement results, i.e. S (−54.76 − −68.80 μV K^{-1}) [27], σ (1526.19–1878.68 S m^{-1}) [27] and κ (0.96–0.72 W m^{-1} K^{-1}), the obtained ZT value of a 75 nm PbTe NW at 300–350 K are in the range of ~1.4–4.3 x 10^{-3} (**Figure 12**) and it is still much lower than the ZT of PbTe bulk which is approximately ~ 0.25 at 300 K and maximal ~ 0.8 at 700 K [42].
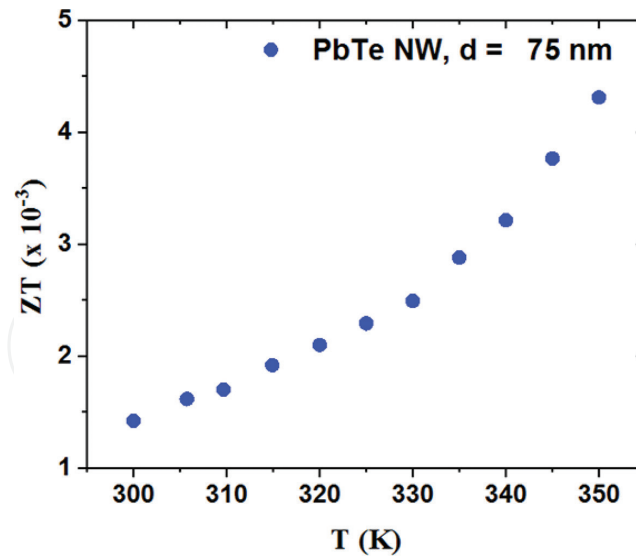
Figure 12. Figure of merit *ZT* for a n-type 75 nm PbTe NW.

4. Conclusions

In summary, we have demonstrated a new technique for structural characterization and TE properties measurement of individual single-crystalline PbTe NW by using a novel design of microchip. In this work, the single PbTe NW grown by the stress-induced method was employed for four different type of characterization simultaneously: structural characterization, Seebeck coefficient, electrical conductivity, and thermal conductivity. The structural characterization revealed that the synthesized PbTe NWs were single crystals with a growth along the [100] direction. While the TE properties (S, σ, and κ) of a 75 nm single-crystalline PbTe NW at room temperature are −54.76 μV K^{-1}, 1526.19 S m^{-1}, and 0.96 W m^{-1} K^{-1}, respectively. Based on those results, the experimental calculation of *ZT* value of its NW was ~1.4–4.3 x 10^{-3} at 300–350 K range. This technique provided high accuracy and reliable ZT value of individual single-crystalline TE NW. Thus, the size-dependent study of TE properties is very feasible. In this study, the κ value in growth [100] direction PbTe NW is size-dependent, wherein indicates that thermal transport through the individual PbTe nanowires is limited by boundary scattering of both electrons and phonons.

Acknowledgements

Conflict of interest

The authors declare no competing conflict of interests.

Author details

Dedi[1,3]*, Indah Primadona[2], Ping-Chung Lee[3], Chi-Hua Chien[3] and Yang-Yuan Chen[3]

*Address all correspondence to: dediamada@yahoo.com

1 Research Center for Electronics and Telecommunication, Indonesian Institute of Sciences, Bandung, Indonesia

2 Research Unit for Clean Technology, Indonesian Institute of Sciences, Bandung, Indonesia

3 Institute of Physics, Academia Sinica, Taipei, Taiwan

References

[1] DiSalvo FJ. Thermoelectric cooling and power generation. Science. 1999;**285**:703-706. DOI: 10.1126/science.285.5428.703

[2] Tritt TM. Thermoelectric materials: Holey and unholey semiconductors. Science. 1999;**283**:804-805. DOI: 10.1126/science.283.5403.804

[3] Dresselhaus MS, Chen G, Tang MY, Yang RG, Lee H, Wang DZ, Ren ZF, Fleurial JP, Gogna P. New directions for low-dimensional thermoelectric materials. Advanced Materials. 2007;**19**:1043-1053. DOI: 10.1002/adma.200600527

[4] Mahan GD. Good thermoelectrics solid state physics. Advances in Research and Applications. 1998;**51**:81-157. DOI: 10.1016/S0081-1947(08)60190-3

[5] Lin YM, Sun X, Dresselhaus MS. Theoretical investigation of thermoelectric transport properties of cylindrical bi nanowires. Physical Review B. 2000;**62**:4610-4623. DOI: 10.1103/PhysRevB.62.4610

[6] Bassi AL, Bailini A, Casari CS, Donati F, Mantegazza A, Passoni M, Russo V, Bottani CE. Thermoelectric properties of Bi–Te films with controlled structure and morphology. Journal of Applied Physics. 2009;**105**:124307(1-9). DOI: 10.1063/1.3147870

[7] Szczech JR, Higgins JM, Jin S. Enhancement of the thermoelectric properties in nanoscale and nanostructured materials. Journal of Materials Chemistry. 2011;**21**:4037-4055. DOI: 10.1039/C0JM02755C

[8] Hicks LD, Dresselhaus MS. Effect of quantum-well structures on the thermoelectric figure of merit. Physical Review B. 1993;**47**:12727-12731. DOI: 10.1103/PhysRevB.47.12727

[9]   Hicks LD, Dresselhaus MS. Thermoelectric figure of merit of a one-dimensional conductor. Physical Review B. 1993;**47**:16631-16634. DOI: 10.1103/PhysRevB.47.16631

[10]   Pei Y, Wang H, Gibbs ZM, LaLonde AD, Snyder GJ. Thermopower enhancement in Pb1−xMnxTe alloys and its effect on thermoelectric efficiency. NPG Asia Materials. 2012;**4**:e28. DOI: 10.1038/am.2012.52

[11]   Rowe DM. CRC Handbook of Thermoelectrics. Boca Raton, FL, USA: CRC Press; 1995. p. 441

[12]   Dughaish ZH. Lead telluride as a thermoelectric material for thermoelectric power generation. Physica B: Condensed Matter. 2002;**322**:205-223. DOI: 10.1016/S0921-4526(02)01187-0

[13]   Heremans JP, Thrush CM, Morelli DT. Thermopower enhancement in lead telluride nanostructures. Physical Review B. 2004;**70**:115334(1-5). DOI: 10.1103/PhysRevB.70.115334

[14]   Heremans JP, Thrush CM, Morelli DT. Thermopower enhancement in PbTe with Pb precipitates. Journal of Applied Physics. 2005;**98**:063703(1-6). DOI: 10.1063/1.2037209

[15]   Orihashi M, Noda Y, Chen LD, Goto T, Hirai T. Effect of tin content on thermoelectric properties of p-type lead tin telluride. Journal of Physics and Chemistry of Solids. 2000;**61**:919-923. DOI: 10.1016/S0022-3697(99)00384-4

[16]   LaLonde AD, Pei Y, Wang H, Snyder GJ. Lead telluride alloy thermoelectrics. Materials Today. 2011;**14**:526-532. DOI: 10.1016/S1369-7021(11)70278-4

[17]   Wei Q, Lieber CM. Synthesis of single crystal bismuth-telluride and lead-telluride nanowires for new thermoelectric materials. Materials Research Society Symposium Proceedings. 2000;**581**:219-223. DOI: 10.1557/PROC-581-219

[18]   Fardy M, Hochbaum AI, Goldberger J, Zhang MM, Yang P. Synthesis and thermoelectrical characterization of lead chalcogenide nanowires. Advanced Materials. 2007;**19**:3047-3051. DOI: 10.1002/adma.200602674

[19]   Roh JW, Jang SY, Kang J, Lee S, Noh JS, Kim W, Park J, Lee W. Size-dependent thermal conductivity of individual single-crystalline PbTe nanowires. Applied Physics Letters. 2010;**96**:103101(1-3). DOI: 10.1063/1.3352049

[20]   Lee SH, Shim W, Jang SY, Roh JW, Kim P, Park J, Lee W. Thermoelectric properties of individual single-crystalline PbTe nanowires grown by a vapor transport method. Nanotech. 2011;**22**:295707(1-6). DOI: https://doi.org/10.1088/0957-4484/22/29/295707

[21]   Yang Y, Taggart DK, Cheng MH, Hemminger JC, Penner RM. High-throughput measurement of the seebeck coefficient and the electrical conductivity of lithographically patterned polycrystalline PbTe nanowires. Journal of Physical Chemistry Letters. 2010;**1**:3004-3011. DOI: 10.1021/jz101128d

[22]   Yang Y, Kung SC, Taggart DK, Xiang C, Yang F, Brown MA, Guell AG, Kruse TJ, Hemminger JC, Penner RM. Synthesis of PbTe nanowire arrays using lithographically

patterned nanowire electrodeposition. Nano Letters. 2008;**8**:2447-2451. DOI: 10.1021/nl801442c

[23] Jung H, Park DY, Xiao F, Lee KH, Choa LH, Yoo B, Myung NV. Electrodeposited single crystalline PbTe nanowires and their transport properties. Journal of Physical Chemistry C. 2011;**115**:2993-2998. DOI: 10.1021/jp110739v

[24] Tai G, Zhou B, Guo W. Structural characterization and thermoelectric transport properties of uniform single-crystalline lead telluride nanowires. Journal of Physical Chemistry C. 2008;**112**:11314-11318. DOI: 10.1021/jp8041318

[25] Tai G, Guo W, Zhang Z. Hydrothermal synthesis and thermoelectric transport properties of uniform single-crystalline pearl-necklace-shaped PbTe nanowires. Crystal Growth & Design. 2008;**8**:2906-2911. DOI: 10.1021/cg701262x

[26] Yan Q, Chen H, Zhou W, Hng HH, Boey FYC, Ma J. A simple chemical approach for PbTe nanowires with enhanced thermoelectric properties. Chemistry of Materials. 2008;**20**:6298-6300. DOI: 10.1021/cm802104u

[27] Dedi, Lee PC, Chien CH, Dong GP, Huang WC, Chen CL, Tseng CM, Harutyunyan SR, Lee CH, Chen YY. Stress-induced growth of single-crystalline lead telluride nanowires and their thermoelectric transport properties. Applied Physics Letters. 2013;**103**:023115(1-5). DOI: 10.1063/1.4813606

[28] Caylor JC, Coonley K, Stuart J, Colpitts T, Venkatasubramanian R. Enhanced thermoelectric performance in PbTe-based superlattice structures from reduction of lattice thermal conductivity. Applied Physics Letters. 2005;**87**:023105(1-3). DOI: 10.1063/1.1992662

[29] Shim W, Ham J, Lee KI, Jeung WY, Johnson M, Lee W. On-film formation of bi nanowires with extraordinary electron mobility. Nano Letters. 2009;**9**:18-22. DOI: 10.1021/nl8016829

[30] Wang D, Sheriff BA, Heath JR. Complementary symmetry silicon nanowire logic: Power-efficient inverters with gain. Small. 2006;**2**:1153-1158. DOI: 10.1002/smll.200600249

[31] Partin DL, Heremans J, Morelli DT, Thrush CM, Olk CH, Perry TA. Growth and characterization of epitaxial bismuth films. Physical Review B: Condensed Matter. 1988;**38**:3818-3824. DOI: 10.1103/PhysRevB.38.3818

[32] Dekuijper AH, Bisschop J. Temperature dependence of concentrations and mobilities in thin bismuth films. Thin Solid Films. 1983;**110**:99-106. DOI: 10.1016/0040-6090(83)90214-6

[33] Horak J, Navratil J, Stary Z. Lattice point defects and free-carrier concentration in $Bi_{2+x}Te_3$ and $Bi_{2+x}Se_3$ crystals. Journal of Physics and Chemistry of Solids. 1992;**53**:1067-1072. DOI: 10.1016/0022-3697(92)90079-S

[34] Dedi, Idayanti N, Lee PC, Lee CH, Chen YY. Thermoelectric power of single crystalline lead telluride nanowire. Journal of Physics Conference Series. 2016;**776**:012046. DOI: 10.1088/1742-6596/776/1/012046

[35] Lu L, Yi W, Zhang D.L. 3ω method for specific heat and thermal conductivity measurements. The Review of Scientific Instruments. 2001;**72**:2996-3003. DOI: 10.1063/1.1378340

[36] Ioffe AF. Semiconductor Thermoelements and Thermoelectric Cooling. London: Infosearch; 1957

[37] Slack GA. The thermal conductivity of nonmetallic crystals. In: Ehreneich H, Seitz F, Turnbull D, editors. Solid State Physics. Vol. 34. New York: Academic Press; 1979. pp. 1-71. DOI: 10.1016/S0081-1947(08)60359-8

[38] Goldsmid HJ. A New Upper Limit to the Thermoelectric Figure-of-Merit. In: Rowe DM, editor. Thermoelectrics Handbook: Macro to Nano. CRC Taylor & Francis; 2006. p. 10.1-10.8

[39] Dames C, Chen G. Thermal Conductivity of Nanostructured Thermoelectric Material. In: Rowe DM, editor. Thermoelectrics Handbook: Macro to Nano. CRC Taylor & Francis; 2006. p. 42.1-42.11

[40] Li D, Wu Y, Kim P, Yang P, Majumdar A. Thermal conductivity of individual silicon nanowires. Applied Physics Letters. 2003;**83**:2934-2936. DOI: 10.1063/1.1616981

[41] Abouelaoualim D. Size effects on nanowire phonon thermal conductivity: A numerical investigation using the Boltzmann equation. Acta Physica Polonica A. 2007;**112**:49-54

[42] Tritt TM, Subramanian MA. Thermoelectric materials, phenomena, and applications: A bird's eye view. MRS Bulletin. 2006;**31**:188-198. DOI: 10.1557/mrs2006.44